Proc. Natl. Acad. Sci. USA
Vol. 88, pp. 2721–2725, April 1991
Neurobiology

Dopa decarboxylase activity of the living human brain

(dopamine/dopamine synthesis/6-[^{18}F]fluoro-L-dopa/Parkinson disease/positron emission tomography)

ALBERT GJEDDE, JAKOB REITH, SUZAN DYVE, GABRIEL LÉGER, MARK GUTTMAN, MIRKO DIKSIC, ALAN EVANS, AND HIROTO KUWABARA

Positron Imaging Laboratories, Montreal Neurological Institute, 3801 University Street, Montreal, Quebec H3A 2B4, Canada

Communicated by Alfred P. Wolf, December 10, 1990 (received for review July 23, 1990)

ABSTRACT **Monoaminergic neurons use dopa decarboxylase (DDC; aromatic-L-amino-acid carboxy-lyase, EC 4.1.1.28) to form dopamine from L-3,4-dihydroxyphenylalanine (L-dopa). We measured regional dopa decarboxylase activity in brains of six healthy volunteers with 6-[^{18}F]fluoro-L-dopa and positron emission tomography. We calculated the enzyme activity, relative to its K_m, with a kinetic model that yielded the relative rate of conversion of 6-[^{18}F]fluoro-L-dopa to [^{18}F]fluorodopamine. Regional values of relative dopa decarboxylase activity ranged from nil in occipital cortex to 1.9 h^{-1} in caudate nucleus and putamen, in agreement with values obtained *in vitro*.**

The accumulation of metabolites of 6-[^{18}F]fluoro-L-dopa (Fdopa) in brain reflects the activity of dopa decarboxylase (DDC; aromatic-L-amino-acid carboxy-lyase, EC 4.1.1.28), the enzyme responsible for the formation of dopamine from dopa (3,4-dihydroxyphenylalanine) (1–3). Unlike tyrosine hydroxylase, this enzyme is believed not to be regulated in response to the intensity of dopaminergic neurotransmission (4). Therefore, DDC activity may be a more precise indicator of the tissue's capacity to synthesize dopamine than tyrosine hydroxylase, the activity of which is adjusted to compensate for changes of dopaminergic activity.

Recently, we used Fdopa to measure the relative activity of DDC *in vivo* in rat brain (5). We defined the relative activity as the ratio between the reaction velocity and the enzyme precursor content of the tissue—i.e., proportional to the ratio between the enzyme's maximal velocity and the half-saturation concentration of precursor when the precursor concentration is negligible relative to the half-saturation Michaelis constant K_m (see Eqs. 7 and 8). In rat brain, the relative enzyme activity was as low as 1% of the relative activity reported *in vitro*. The reason for the discrepancy was unknown, but we speculated that it most probably was the loss of labeled fluorodopamine or its metabolites from one or more pools of dopamine in the tissue.

In the present study, we obtained the relative activity of DDC in human brain *in vivo*. *In vitro*, the monoamine oxidase activities are lower in human brain than in rat brain (see *Discussion*), and metabolite diffusion distances are longer. For these reasons, we predicted the human relative DDC activity, determined in striatum *in vivo* with positron emission tomography (PET), to be close to the relative rate of dopamine synthesis determined *in vitro*.

METHODS

A model of the transport and metabolism of Fdopa in brain *in vivo* must include the compartments and transfer coefficients shown in Fig. 1. The model describes the methylation of Fdopa in the circulation (actually in peripheral organs), the loss of methyl-Fdopa from the circulation, the methylation of Fdopa in brain tissue, the exchange of Fdopa and methyl-Fdopa between the circulation and brain tissue, and the decarboxylation of Fdopa in the tissue. The model has too many compartments to be evaluated by PET. We used known relationships between the parameters to reduce the number of compartments to three and the number of parameters to four: We incorporated into each study (*i*) the ratio (0.43) between the blood–brain barrier transport rates of Fdopa and methyl-Fdopa in rat (5), (*ii*) the rate of conversion of Fdopa to methyl-Fdopa and the rate of loss of methyl-Fdopa from the circulation, and (*iii*) judgment that k_5^D, the rate coefficient of methylation in brain tissue, was small compared with k_o^D, the whole-body rate coefficient of methylation.

Determination of k_o^D. For first-order processes of methylation and elimination, the concentration of methyl-Fdopa in the circulation is given by the equation

$$\frac{dC_a^M(t)}{dt} = k_o^D C_a^D(t) - k_{-1}^M C_a^M(t), \quad [1]$$

where $C_a^M(t)$ is the methyl-Fdopa concentration, k_o^D is the coefficient of methylation, $C_a^D(t)$ is the plasma concentration of Fdopa, and k_{-1}^M is the coefficient of methyl-Fdopa clearance from the circulation. Following integration and division, we obtained a linear equation with k_o^D as the slope and $-k_{-1}^M$ as the ordinate intercept,

$$\frac{C_a^M(T)}{\int_0^T C_a^M(t)dt} = k_o^D \frac{\int_0^T C_a^D(t)dt}{\int_0^T C_a^M(t)dt} - k_{-1}^M, \quad [2]$$

where T is a time point, and t is a time variable.

Determination of V_e. In the absence of metabolic or other trapping of the tracer, the distribution between the circulation and the tissues is governed by the rate of blood–tissue clearance, K_1, and the relative rate of tissue–blood clearance, k_2. The tracer Fdopa partition volume V_e, equal to the K_1/k_2 ratio, was determined in the lowest of the three planes of radioactivity registered by the tomograph, which included no striatal structures. In the absence of decarboxylation or O-methylation of Fdopa in brain, the extravascular Fdopa content is determined by

$$\frac{dM_e^D(t)}{dt} = K_1^D C_a^D(t) - k_2^D M_e^D(t), \quad [3]$$

The publication costs of this article were defrayed in part by page charge payment. This article must therefore be hereby marked "*advertisement*" in accordance with 18 U.S.C. §1734 solely to indicate this fact.

Abbreviations: dopa, 3,4-dihydroxyphenylalanine; DDC, dopa decarboxylase; Fdopa, 6-[^{18}F]fluoro-L-dopa; PET, positron emission tomography.

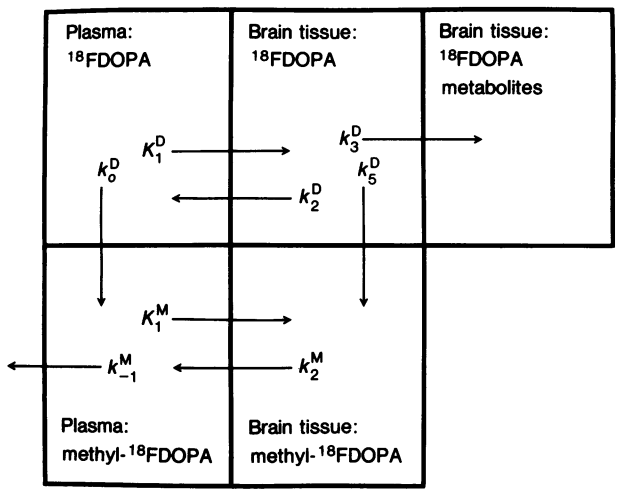

FIG. 1. Transport and metabolism of Fdopa in a five-compartment model of the brain. The total radioactivity in a region is distributed between three compartments: intravascular space, extravascular tissue (precursor pool), and metabolite compartment (metabolically trapped tracer). The model includes eight transfer coefficients. The coefficient of brain tissue methylation of Fdopa, k_5^D, was assumed to be negligible compared with the coefficient of extracerebral methylation. Because of the 2-h half-life of dopamine in brain, this model included no loss of fluorodopamine metabolites from brain.

where $M_e^D(t)$ is the extravascular Fdopa content of the tissue. Likewise, the extravascular content of methyl-Fdopa is determined by

$$\frac{dM_e^M(t)}{dt} = K_1^M C_a^M(t) - k_2^M M_e^M(t), \qquad [4]$$

where $M_e^M(t)$ is the methyl-Fdopa content of the tissue. With the introduction of the constant q, the ratio between K_1^M and K_1^D, which is equal to the ratio between k_2^M and k_2^D, we obtained

$$\frac{dM_e^M(t)}{dt} = qK_1^D C_a^M(t) - qk_2^D M_e^M(t). \qquad [5]$$

The combined solution to Eqs. 3 and 5 is

$$M^*(T) = K_1^D e^{-[K_1^D/V_e]T} \times \int_0^T C_a^D(t) e^{[K_1^D/V_e]t} dt + qK_1^D e^{-[qK_1^D/V_e]T} \times \int_0^T C_a^M(t) e^{[qK_1^D/V_e]t} dt + V_o C_a^*(T), \qquad [6]$$

where $M^*(T)$ is the total extravascular radioactivity, V_o is the initial volume of distribution, and $C_a^*(T)$ is the total arterial concentration of radioactivity. The equation has three unknowns, K_1^D, V_o, and V_e when the values of q, $C_a^*(T)$, $C_a^D(t)$, $C_a^M(t)$, and $M^*(T)$ are known.

Determination of k_3^D. In a region of brain that traps the tracer Fdopa only by decarboxylation, the relative activity of DDC towards native dopa is

$$k_3 = \frac{v}{M_e} = \frac{V_{max}}{K_m\left(V_d + \sum_{i=1}^{n} \frac{M_i}{K_i}\right)}, \qquad [7]$$

where V_{max} is the maximal velocity of the native decarboxylation reaction *in vivo*, v is the velocity of native dopamine synthesis *in vivo*, M_e is the native dopa content of the tissue, K_m is the Michaelis half-saturation concentration of native dopa, V_d is the water volume of brain tissue (assumed to be the distribution volume for Fdopa), M_i represents the contents of n inhibitors in the tissue (including dopa and Fdopa), and K_i represents the inhibitory constant of the n inhibitors.

The definition of k_3^D for Fdopa is

$$k_3^D = \frac{V_{max}^D}{K_m^D\left(V_d + \sum_{i=1}^{n} \frac{M_i}{K_i}\right)} = k_3\left(\frac{K_m V_{max}^D}{K_m^D V_{max}}\right), \qquad [8]$$

where V_{max}^D is the maximal velocity of the tracer reaction *in vivo*, and K_m^D is the Michaelis half-saturation concentration of the tracer. Hence, the decarboxylase activity toward Fdopa is linearly proportional to the activity toward native dopa.

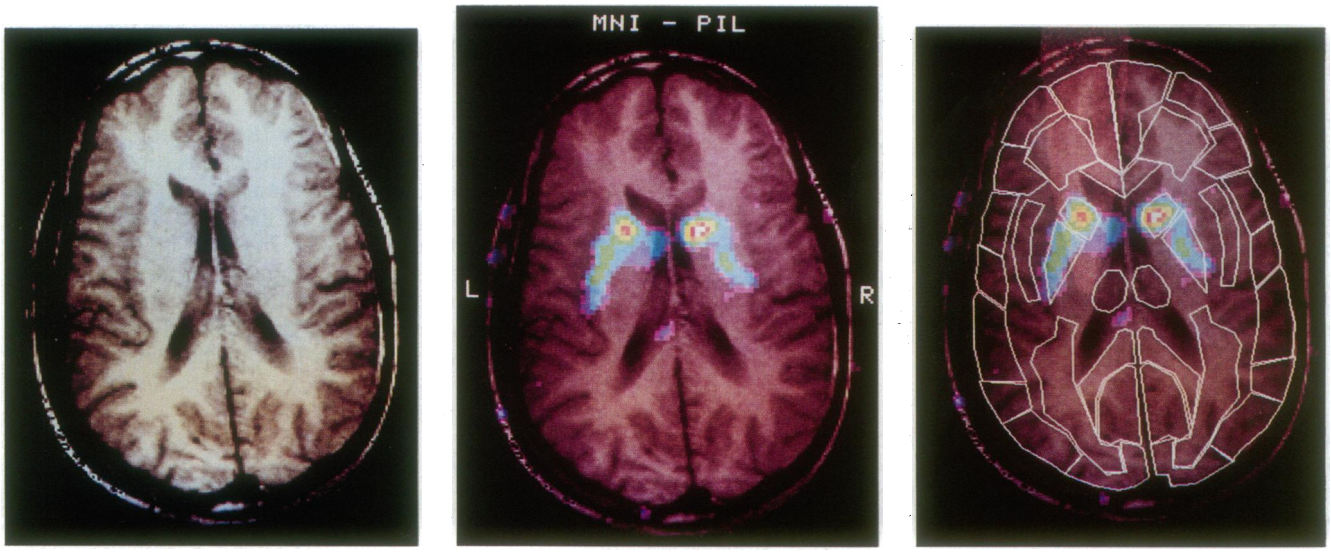

FIG. 2. (*Left*) Axial magnetic resonance image through the striatum, 5.2 cm above and parallel to the orbito-meatal line in a normal subject. (*Center*) PET image of Fdopa-derived radioactivity in same plane, merged with magnetic resonance image by using known landmarks of the skull. (*Right*) Regions of interest in the corresponding magnetic resonance image plane (see *Left*).

When the metabolism of Fdopa is irreversible and metabolites do not leave the brain tissue, the accumulated metabolites of Fdopa are given by the solution of the equation

$$\frac{dM_m^D(t)}{dt} = k_3^D M_e^D(t), \quad [9]$$

where $M_m^D(t)$ is the regional content of Fdopa metabolites. The extravascular content of Fdopa is given by

$$\frac{dM_e^D(t)}{dt} = K_1^D C_a^D(t) - (k_2^D + k_3^D) M_e^D(t), \quad [10]$$

where $C_a^D(t)$ is the arterial plasma concentration. The extravascular content of methyl-Fdopa is given by Eqs. **3** and **5**. We show below that k_o^D, the whole-body coefficient of methylation, is so small that it is valid to assume that k_5^D is insignificant compared with k_3^D. The solution of Eqs. **5**, **9**, and **10** for the total content of tracers in a region of brain, when V_e is known, is:

$$M^*(T) = \left(\frac{K_1^D}{K_1^D + k_3^D V_e}\right)\left[k_3^D V_e \int_0^T C_a^D dt + K_1^D e^{-([K_1^D/V_e]+k_3^D)T} \times \int_0^T C_a^D e^{([K_1^D/V_e]+k_3^D)t} dt\right] + qK_1^D e^{-q[K_1^D/V_e]T} \int_0^T C_a^M e^{q[K_1^D/V_e]t} dt + V_0 C_a^*(T). \quad [11]$$

This equation has three unknowns, K_1^D, V_0, and k_3^D, when $M^*(T)$, $C_a^D(t)$, $C_a^M(t)$, $C_a^*(T)$, V_e, and q are known.

Procedures. The subjects included six healthy 19- to 42-year-old volunteers (mean age, 28 years), studied in accordance with an experimental protocol approved by the Ethics Committee of the Montreal Neurological Institute and Hospital.

Informed consent was obtained after full explanation of the nature and possible consequences of the studies. The subjects were treated with 100 mg of carbidopa 1 h before the study to inhibit peripheral decarboxylation of Fdopa to fluorodopamine and were injected with 5 mCi (1 Ci = 37 GBq) of Fdopa, which circulated for 120 min. At a specific activity of 300 mCi·mmol^{-1}, the mass of Fdopa was 17 μmol. When dissolved in 50 liters of body water, the intracellular concentration of Fdopa did not exceed 0.3 μM, or <1% of the K_m for DDC. Arterial blood samples were obtained as rapidly as possible between 0 and 5 min (average, 17 samples), every 5 min between 10 and 25 min, at 35 min, and every 15 min between 45 and 120 min. Plasma samples for HPLC were obtained every 5 min between 5 and 35 min and at 45, 60, and 90 min thereafter. During this time, three planes of dynamic (90 min) and static (30 min) images were acquired with the Therascan-3128 scanner, a three-plane tomograph with a 12-mm transverse by 12-mm axial spatial resolution (6).

In the PET images, anatomical regions were identified in a computerized atlas of the human brain, with the aid of magnetic resonance images obtained in association with the PET images, by the method of Evans *et al.* (7). In three subjects, the three planes were acquired 23 ± 6, 35 ± 6, and 47 ± 6 mm (mean ± SD) above the orbito-meatal line. In the three remaining subjects, the three planes were interleaved at 31 ± 2, 43 ± 2, and 55 ± 2 mm above the orbito-meatal line.

The regionally recorded radioactivities were fitted by Eq. **6** or **11** and yielded values of plasma volume (V_o), blood-brain clearance (K_1^D), and partition volume (V_e, lowest of three planes in all subjects) or relative DDC activity (k_3^D, higher two planes in all subjects) (Fig. 1). The coefficient of peripheral methylation, k_o^D, was determined by HPLC analysis. Arterial blood time–radioactivity curves of total radioactivity, Fdopa radioactivity, and methyl-Fdopa radioactivity were established on the basis of the arterial samples and the HPLC measurements. The synthesis of Fdopa and the HPLC analysis of Fdopa and metabolites in plasma have been described in detail (5). Carbidopa was a gift from Merck.

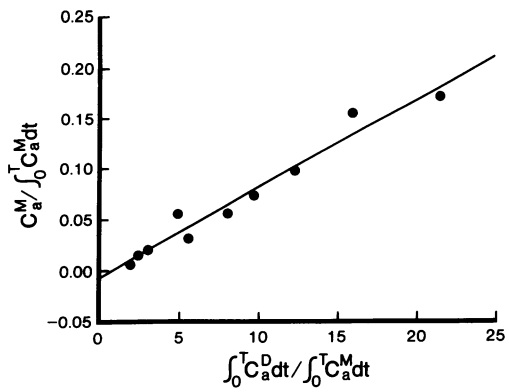

FIG. 3. Representative graph of linear Eq. **2**. The abscissa (a ratio) has no units; the ordinate has a unit of inverse time (min^{-1}). The slope yielded an estimate of methylation coefficient k_o^D, and the ordinate intercept yielded a negative estimate of the elimination coefficient k_1^M.

RESULTS

Representative magnetic resonance and PET image planes of one subject are shown in Fig. 2 *Left* and *Right*. The regions outlined in Fig. 2 *Right* were identified from a computerized atlas applied to the magnetic resonance image shown in Fig. 2 *Left*.

Determination of k_o^D. The rate constant of conversion of Fdopa to methyl-Fdopa—i.e., the relative catechol-*O*-methyltransferase activity—k_o^D, was calculated from Eq. **2** as exemplified for one subject in Fig. 3. The slope, k_o^D, averaged

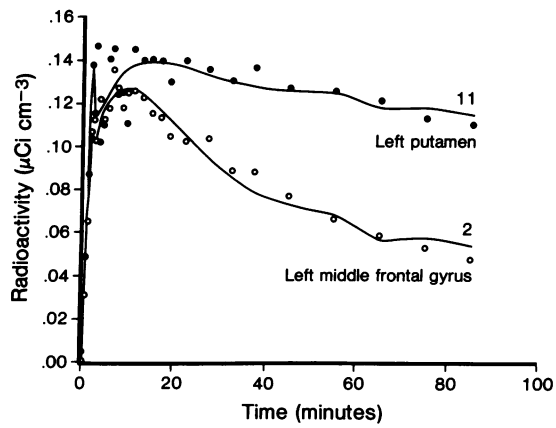

FIG. 4. Radioactivity recorded in two regions of the plane of subject shown in Fig. 2 after i.v. injection of 5 mCi of Fdopa. Region 2 is the left middle frontal gyrus, and region 11 is the left putamen. In this example, k_o averaged 0.66 h^{-1}. By using the values q = 2.3 and V_e = 0.40 ml·cm^{-3}, the radioactivity recorded in the two regions was subjected to nonlinear least-squares regression analysis by Eq. **11**. The lines were drawn on the basis of the parameter estimates. The F statistics of the fits were 1729 and 1432. The estimates of K_1^D were 1.5 ml·cm^{-3}·h^{-1} in both regions, the estimate of V_o was 0.03 ml·cm^{-3} in both the left middle frontal gyrus and the left putamen, and the estimates of k_3^D were 0.0 h^{-1} in the left middle frontal gyrus and 1.4 h^{-1} in the left putamen.

$0.54 \pm 0.04\ h^{-1}$ (mean ± SEM). The ordinate intercept, the rate constant for elimination of methyl-Fdopa from the circulation, $-k_{-1}^{M}$, averaged $-0.36 \pm 0.36\ h^{-1}$ and hence was insignificantly different from zero. The magnitude of k_o^D suggested that the magnitude of k_5^D, the coefficient of methylation in brain tissue, is of the order of $0.05\ h^{-1}$, or <5% of the magnitude of k_3^D in caudate nucleus and putamen.

Determination of V_e. Using the predetermined value of q (2.3; ref. 5), we estimated the value of V_e in the lowest two planes of the tomographic images (23 ± 6 and 31 ± 2 mm above the orbito-meatal line). The average value of the six brains was $0.52 \pm 0.06\ ml \cdot cm^{-3}$ (mean ± SEM). The corresponding estimate of K_1 was $1.68 \pm 0.18\ ml \cdot cm^{-3} \cdot h^{-1}$ (mean ± SEM).

Determination of k_3^D. We used the value of V_e determined for each subject to estimate the regional values of K_1^D, the blood–brain clearance of Fdopa, and k_3^D, the coefficient of metabolism of Fdopa, by means of Eq. **11**. The analysis of two regions of the same plane from a single subject is shown in Fig. 4. The results for all regions of interest are listed in Table 1. Results obtained in the lowest planes were not listed because these were used to determined V_e, as explained above.

Table 1 includes the average distance of a given tomographic plane from the orbito-meatal line, the volume of

Table 1. *In vivo* estimates of relative DDC activity in human brain

Region	Plane above OM line, cm	Hemisphere	Sample volume, cm^3	K_1^D, $ml \cdot cm^{-3} \cdot h^{-1}$	k_3^D, h^{-1}
Amygdala	3.5 ± 0.6	L	1.7 ± 0.1	1.5 ± 0.2	0.5 ± 0.01
		R	1.7 ± 0.1	1.5 ± 0.1	0.5 ± 0.1
Midbrain	3.5 ± 0.6	L	2.2 ± 0.1	1.8 ± 0.1	0.4 ± 0.3
		R	2.3 ± 0.1	1.7 ± 0.2	0.5 ± 0.3
	4.3 ± 0.2	L	4.3 ± 0.2	1.2 ± 0.3	0.2 ± 0.01
		R	4.3 ± 0.1	1.1 ± 0.3	0.1 ± 0.01
Hippocampus	3.5 ± 0.6	L	1.7 ± 0.1	1.6 ± 0.2	0.5 ± 0.1
		R	1.7 ± 0.1	1.4 ± 0.2	0.2 ± 0.01
	4.3 ± 0.2	L	3.1 ± 0.1	1.0 ± 0.2	0.0 ± 0.0
		R	2.7 ± 0.2	0.9 ± 0.2	0.0 ± 0.0
	4.7 ± 0.6	L	2.1 ± 0.1	1.6 ± 0.2	0.1 ± 0.1
		R	1.9 ± 0.1	1.4 ± 0.3	0.1 ± 0.1
Inferior temporal gyrus	3.5 ± 0.6	L	5.4 ± 0.4	1.4 ± 0.3	0.0 ± 0.0
		R	5.6 ± 0.3	1.5 ± 0.3	0.0 ± 0.0
	4.3 ± 0.2	L	4.7 ± 0.2	1.3 ± 0.3	0.0 ± 0.0
		R	4.8 ± 0.2	1.2 ± 0.3	0.0 ± 0.0
	4.7 ± 0.6	L	6.7 ± 0.2	1.8 ± 0.3	0.1 ± 0.1
		R	6.8 ± 0.1	1.7 ± 0.3	0.1 ± 0.1
	5.5 ± 0.2	L	6.0 ± 0.2	1.3 ± 0.2	0.0 ± 0.0
		R	6.2 ± 0.3	1.3 ± 0.2	0.0 ± 0.0
Caudate nucleus	4.3 ± 0.2	L	0.8 ± 0.2	1.1 ± 0.3	0.8 ± 0.4
		R	0.9 ± 0.4	1.2 ± 0.2	0.8 ± 0.4
	4.7 ± 0.6	L	1.7 ± 0.02	1.5 ± 0.1	1.9 ± 0.4
		R	1.9 ± 0.1	1.4 ± 0.1	1.5 ± 0.1
	5.5 ± 0.2	L	2.1 ± 0.1	1.1 ± 0.2	1.6 ± 0.2
		R	2.0 ± 0.1	1.0 ± 0.2	1.6 ± 0.3
Putamen	4.3 ± 0.2	L	2.4 ± 0.5	1.1 ± 0.3	0.8 ± 0.5
		R	2.7 ± 0.5	1.1 ± 0.3	0.7 ± 0.4
	4.7 ± 0.6	L	5.5 ± 0.2	2.2 ± 0.3	1.9 ± 0.2
		R	5.8 ± 0.3	2.0 ± 0.4	1.8 ± 0.3
	5.5 ± 0.2	L	4.2 ± 0.4	1.4 ± 0.2	1.9 ± 0.3
		R	4.5 ± 0.2	1.3 ± 0.2	1.6 ± 0.1
Superior frontal gyrus	4.3 ± 0.2	L	9.4 ± 0.3	1.2 ± 0.1	0.0 ± 0.0
		R	8.8 ± 0.4	1.1 ± 0.1	0.0 ± 0.0
	4.7 ± 0.6	L	7.8 ± 0.1	1.5 ± 0.3	0.1 ± 0.1
		R	7.8 ± 0.1	1.6 ± 0.2	0.3 ± 0.1
	5.5 ± 0.2	L	7.2 ± 0.1	1.0 ± 0.2	0.0 ± 0.0
		R	7.3 ± 0.1	1.1 ± 0.2	0.0 ± 0.0
Middle occipital lobe	4.3 ± 0.2	L	3.5 ± 0.2	1.8 ± 0.6	0.0 ± 0.0
		R	3.6 ± 0.1	1.8 ± 0.4	0.0 ± 0.0
	4.7 ± 0.6	L	2.4 ± 0.1	1.6 ± 0.4	0.0 ± 0.0
		R	2.3 ± 0.1	1.6 ± 0.3	0.0 ± 0.0
	5.5 ± 0.2	L	2.6 ± 0.1	1.5 ± 0.4	0.0 ± 0.0
		R	2.5 ± 0.2	1.6 ± 0.4	0.0 ± 0.0
Thalamus	4.7 ± 0.6	L	4.8 ± 0.1	2.0 ± 0.3	0.4 ± 0.1
		R	5.0 ± 0.3	1.9 ± 0.2	0.3 ± 0.1
	5.5 ± 0.2	L	5.8 ± 0.2	1.2 ± 0.3	0.1 ± 0.1
		R	5.3 ± 0.2	1.2 ± 0.3	0.0 ± 0.0
Posterior occipital lobe	5.5 ± 0.2	L	4.4 ± 0.2	1.9 ± 0.8	0.0 ± 0.0
		R	4.5 ± 0.2	1.7 ± 0.5	0.0 ± 0.0

OM, orbital-meatal; L, left; R, right.

tissue sampled assuming a plane thickness of 12 mm, the unidirectional clearance of the tracer from the circulation to brain tissue (K_1^D), and the DDC activity (k_3^D) estimated for the regions of interest named in the left-most column. The volume of tissue sampled was determined from the area of the regional outline selected for analysis and the thickness of the plane from which the tissue radioactivity was acquired (i.e., 12 mm).

The volume of tissue sampled varied from 9.4 cm^3 of the superior frontal gyrus to 0.9 cm^3 of the caudate nucleus, assuming a uniform width of 12 mm of the regional section. The blood–brain clearances of Fdopa (K_1^D) had moderate regional variation, with the highest value (2.2 $ml \cdot cm^{-3} \cdot h^{-1}$) recorded in the putamen and the lowest value (0.9 $ml \cdot cm^{-3} \cdot h^{-1}$) recorded in the hippocampus. The relative DDC activity was highest in the caudate nucleus and putamen (1.9 h^{-1}) and lowest in the occipital lobe (≈ 0). The average value in caudate nucleus was at least 20-fold higher than the relative enzyme activity determined in the superior frontal gyrus. The highest extrastriatal activity was registered in the amygdala, midbrain, and hippocampus (0.5 h^{-1}).

DISCUSSION

The interpretation of PET images obtained with labeled Fdopa has been difficult as a result of the complexity of labeled Fdopa membrane transport and metabolism, particularly the formation of 3-*O*-methyl-[^{18}F]fluorodopa of which no previous model took complete account.

One approach has been to calculate an "influx" constant, representing the net clearance of Fdopa from the circulation to brain tissue during steady state, combining several independent physiological processes, including transport across the blood–brain barrier, competition for transport by other amino acids, uptake into neurons, decarboxylation to fluorodopamine, and trapping within neuronal vesicles (8, 9). Native dopa is generated in monoaminergic neurons by the action of tyrosine hydroxylase. Tracer Fdopa enters monoaminergic neurons and other brain cells that possess DDC from the circulation. The biochemical path shared by the two compounds begins with decarboxylation. Therefore, the calculation of the tracer's unidirectional clearance from the circulation yields no information relevant to the metabolism of the native substrate. The influx constant or net clearance does not distinguish between the individual physiological processes involved in the uptake and metabolism of Fdopa. Hence, changes of the net clearance of Fdopa may reflect changes that do not affect the decarboxylation of native dopa directly, including inhibition of blood–brain Fdopa transfer by large neutral amino acids in the circulation.

In theory, the present method yielded an estimate of the velocity of a biochemical step common to tracer and native substrate. We assume that the specific process traced by labeled Fdopa metabolites must be DDC because it is the first irreversible reaction that Fdopa meets. Several factors may contribute to a lowering of the calculated value of the relative enzyme activity, including (*i*) the partial volume effect and (*ii*) the loss of labeled metabolites by diffusion and transport from regions of interest.

First, the finite resolution of the imaging system used (12 mm × 12 mm × 12 mm) resulted in systematic loss of signal from smaller structures—i.e., the partial volume effect (10–12). For isolated structures of high radioactivity, this reduces the amplitude but not the shape of the time–radioactivity curve. The result is decreases of K_1 and V_0 but not of k_2 and k_3. Partial volume effects for large isolated "hot spots," such as the striatum, are of secondary importance. For smaller structures, the contamination from neighboring tissue will be significant, and the resultant k_3 may be an underestimate of DDC activity in the amygdala and hippocampus.

Second, a fraction of newly formed dopamine is subject to very rapid breakdown by monoamine oxidase, the activity of which is so high that little free dopamine is likely to exist outside the storage vesicles of monoaminergic terminals. In rodent striatum, the activity of monoamine oxidase A is 120 $\mu mol \cdot g^{-1} \cdot h^{-1}$, indicating a concentration of dopamine available for oxidation (e.g., the dopamine outside vesicles) of no more than 30 nM at the rate of dopamine turnover determined in rodent striatum. Hence, the half-life of intracellular free dopamine may be no more than 2 s (13). This deduction suggests that only labeled fluorodopamine stored in vesicles remains *in situ* sufficiently long to be recorded by PET. The significance of the rapid breakdown depends, of course, on the speed with which labeled metabolites escape from the regions of interest and on the fraction of fluorodopamine not protected from immediate metabolism by incorporation into vesicles. In rat, *in vivo* estimates of relative DDC activity using the present model and manual tissue sampling suggested that as little as 1% of newly formed dopamine entered vesicles or remained otherwise protected from rapid metabolism.

In the humans studied here, however, the relative DDC activities determined in striatum and surrounding cortical regions agree reasonably well with the *in vitro* measurements (14–17). The good correlation indicates that Fdopa, in humans, is converted to metabolites that leave the regions of interest slowly. In rat, as much as 86% of total dopamine oxidation (monoamine oxidases A and B) in caudate nucleus takes place intraneuronally, whereas in humans, only 18% of total dopamine oxidation in caudate nucleus is intraneuronal (18). Also, total monoamine oxidase activity in human caudate, measured *in vitro*, is 1–10 $\mu mol \cdot g^{-1} \cdot h^{-1}$ (17, 19) or at least 1 order of magnitude less than the monoamine oxidase activity of rat striatum.

This work was supported by the Medical Research Council of Canada (PG-41, SP-30), by the Lundbeck Foundation (Copenhagen), and by fellowships from the Jeanne Timmins Costello Fund (to S.D.) and the Human Frontier Science Program (to J.R.).

1. Garnett, E. S., Firnau, G., Chan, P. K. H., Sood, S. & Belbeck, L. W. (1978) *Proc. Natl. Acad. Sci. USA* **75**, 464–467.
2. Garnett, E. S., Firnau, G. & Nahmias, C. (1983) *Nature (London)* **305**, 137–138.
3. Firnau, G., Sood, S., Chirakal, R., Nahmias, C. & Garnett, E. S. (1987) *J. Neurochem.* **48**, 1007–1082.
4. Lovenberg, W. & Victor, S. J. (1974) *Life Sci.* **14**, 2337–2353.
5. Reith, J., Dyve, S., Kuwabara, H., Guttman, M., Diksic, M. & Gjedde, A. (1990) *J. Cereb. Blood Flow Metab.* **10**, 707–719.
6. Cooke, B. E., Evans, A. C., Fanthome, E. O., Alarie, R. & Sendyk, A. M. (1984) *IEEE Trans. Nucl. Sci.* **31**, 640–644.
7. Evans, A. C., Beil, C., Marrett, S., Thompson, C. J. & Hakim, A. (1988) *J. Cereb. Blood Flow Metab.* **8**, 513–530.
8. Leenders, K. L., Poewe, W. H., Palmer, A. J., Brenton, D. P. & Frackowiak, R. S. J. (1986) *Ann. Neurol.* **20**, 258–262.
9. Martin, W. R. W., Palmer, M. R., Patlak, C. S. & Calne, D. B. (1989) *Ann. Neurol.* **26**, 535–542.
10. Hoffman, E. J., Huang, S. C. & Phelps, M. E. (1979) *J. Comput. Assist. Tomogr.* **3**, 299–308.
11. Mazziotta, J. C., Phelps, M. E., Plummer, D. & Kuhl, D. E. (1981) *J. Comp. Assist. Tomogr.* **5**, 734–743.
12. Kessler, R. M., Ellis, J. R. & Eden, M. (1984) *J. Comput. Assist. Tomogr.* **8**, 514–522.
13. Schoepp, D. D. & Azzaro, A. J. (1981) *J. Neurochem.* **36**, 2025–2031.
14. Lloyd, K. & Hornykiewicz, O. (1972) *J. Neurochem.* **19**, 1549–1559.
15. Sharpe, J. A., Rewcastle, N. B., Lloyd, K. G., Hornykiewicz, O., Hill, M. & Tasker, R. R. (1973) *J. Neurol. Sci.* **19**, 275–286.
16. McGeer, P. L. & McGeer, E. G. (1976) *J. Neurochem.* **26**, 65–76.
17. Mackay, A. V. P., Davies, P., Dewar, A. J. & Yates, C. M. (1978) *J. Neurochem.* **30**, 827–839.
18. Oreland, L., Yuichiro, A. & Stenstrom, A. (1983) *Acta Neurol. Scand.* **95**, 81–85.
19. Riederer, P. & Jellinger, K. (1983) *Acta Neurol. Scand.* **95**, 43–55.